Proceedings of the IASS 2024 Symposium
Redefining the Art of Structural Design
August 26-30, 2024, Zurich Switzerland
Philippe Block, Giulia Boller, Catherine DeWolf,
Jacqueline Pauli, Walter Kaufmann (eds.)

Wind load analysis of a series of arch-supported membrane structures

Krisztián HINCZ*, Sherly Joanna POOL-BLANCO[a], Richárd Joao ROSA[a], Márton KOREN[b], Márton BALCZÓ[b]

*[a] Department of Structural Mechanics, Faculty of Civil Engineering,
Budapest University of Technology and Economics
Műegyetem rkp. 3., Kmf. 63., Budapest, Hungary
* hincz.krisztian@emk.bme.hu

[b] Department of Fluid Mechanics, Faculty of Mechanical Engineering,
Budapest University of Technology and Economics

Abstract

Determining the wind load on tensile membrane structures is a more complex task than in the case of structures with conventional shapes. Design standards typically have no or minimal specifications for tensile membrane structure's very diverse double curvature surfaces. The most reliable way to determine the wind load effects is the measurement of pressures on a scaled model in a wind tunnel. With the development of numerical methods and computers, Computational Fluid Dynamics (CFD) calculations are increasingly a possible alternative for determining the wind load on the surface of the structures.

The research aimed to determine the pressure distribution on the surface of a series of arch-supported membrane structures with a close to hemicylindrical shape with the help of both above-mentioned methods. The wind tunnel experiments were completed at the Theodore von Kármán Wind Tunnel Laboratory of the Budapest University of Technology and Economics. The wind pressure coefficient distributions and the wind force coefficients acting on the rigid model immersed in a boundary layer flow were determined for various wind directions. The CFD calculations were completed with the help of Ansys Fluent. The Reynolds-averaged Navier-Stokes (RANS) approach was applied for the numerical analysis of the flow. The CFD-based mean pressure coefficient values were statistically compared with the experimental values.

Keywords: tensile membrane structures, wind load, wind tunnel test, computational fluid dynamics, pressure coefficient, wind force coefficient.

1. Introduction

Tensile membrane structures are aesthetic and economical structures. However, their design is significantly different from traditional structures. Special procedures are required, from form-finding through the determination of cutting patterns to structural analysis (Barnes [1], Hincz [2]). Determining the wind load on the membrane's surface is also a complex problem because the design standards do not provide the pressure coefficient maps for the anticlastic surface of tensile membrane structures. The European Standard: Temporary structures - Tents – Safety [3] gives two oversimplified load cases for tensile membranes with constant wind pressure and constant wind suction on the whole roof regardless of the shape of the surface. During the design, the pressure distribution on a specific structure can be determined based on Wind Tunnel Tests (WTT), numerical CFD analysis, or previous WTT results on similar shapes. The European Design Guide for Tensile Surface Structures (Forster and Mollaert [4]) presents the pressure distributions for typical membrane shapes and various open stadium roofs. Hoxey

and Richardson [5] introduce the pressure values measured on the surface of full-scale, arch-supported, plastic film-covered greenhouses. Rizzo et al. [6] compared various analytical solutions of wind load on hyperbolic roofs with experimental results. Sun et al. [7] present the WTT-based wind pressure distribution of oval-shaped arch-supported membrane structures. The pressure measurements during wind tunnel tests are typically completed on rigid models. Hincz and Gamboa-Marrufo [8] analysed the effects of the deformations of the membrane roof on the wind pressure distribution in the case of a mast-supported membrane structure.

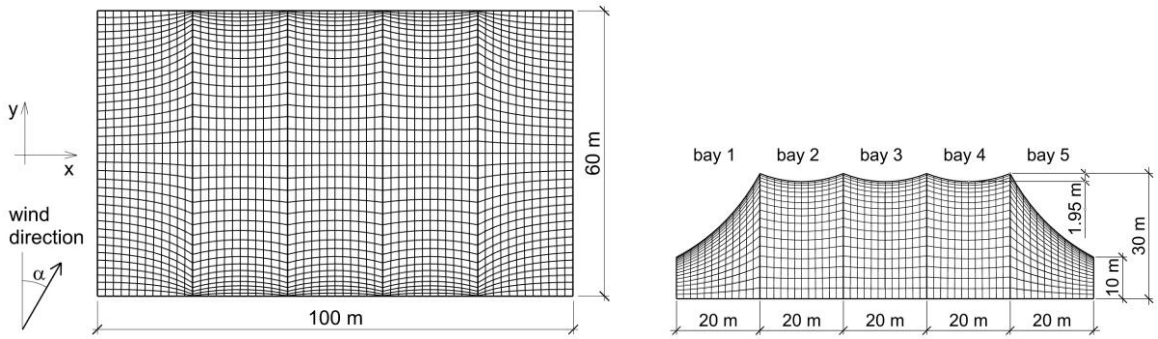

Figure 1: Top and side view of the 5-bay structure

The current study aimed to determine the pressure distribution on the surface of tensile membrane structures supported by circular arches. The anticlastic surfaces of the analysed tensile roofs were approximated with meshes of planar triangular membrane elements; the equilibrium shapes were determined by the Dynamic Relaxation Method (Day [9]). Models with 3, 4 and 5 bays, supported by 4, 5 and 6 arches, were analysed by WTT and CFD. The sizes of the largest analysed structure can be seen in Figure 1, and all models are presented in Figure 2.

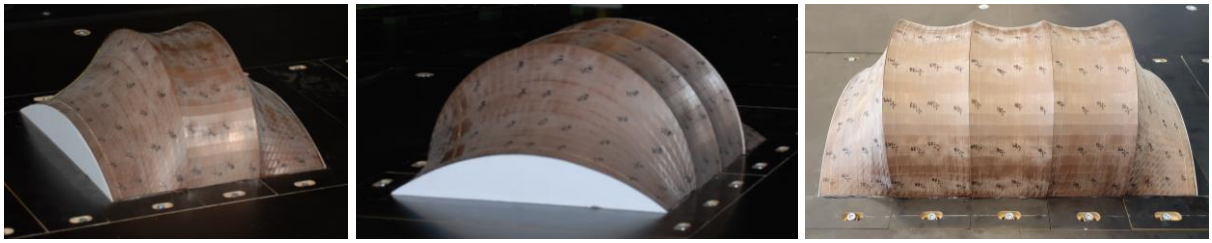

Figure 2: Models with 3, 4 and 5 bays

2. Wind tunnel measurements

2.1. The model

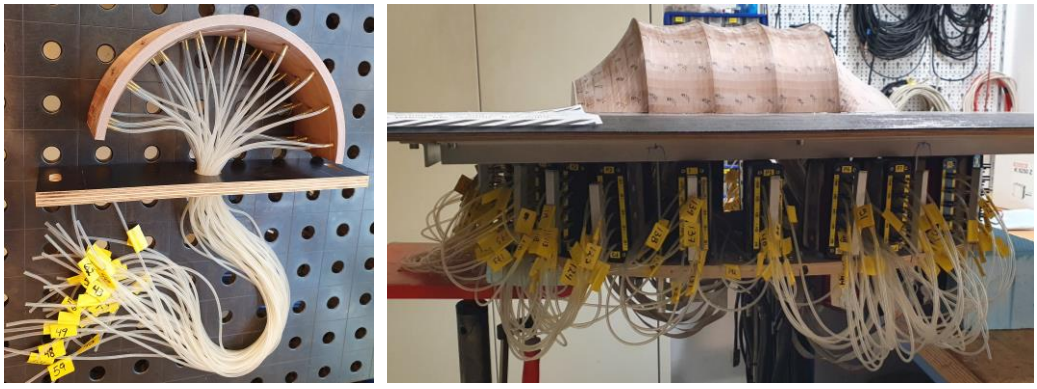

Figure 3: Phases of model making

Five modules were 3D printed on a scale of 1:250 for the longest structure; in the case of the 4 and 3-bay models, 1 or 2 modules were removed from the middle. The model was closed with two thin plastic end walls. 36 (4 × 9) pressure taps were made on the surface of all five modules, which means 180 taps for the longest model. Copper tubes with an internal diameter of 0.9 mm were glued into the holes. The copper tubes are connected to the pressure measuring equipment by 750 mm long, 1.0 mm inner diameter silicone tubing (Figure 3). The distortion of pressure signals due to the long tubing was compensated for during data postprocessing. The applied simultaneous pressure measurement system uses temperature-compensated, amplified Honeywell HSC pressure sensors with +/- 500 Pa measurement range, +/- 2.5 Pa accuracy and analogue output.

2.2. The wind tunnel test

The WTT was completed at the Theodore von Kármán Wind Tunnel Laboratory of the Budapest University of Technology and Economics. The wind tunnel is of horizontal closed-return type with an open test section. The wind tunnel model was placed on a horizontal turntable, allowing the model to rotate to simulate any desired wind direction. The atmospheric boundary layer (ABL) in the model scale (M=1:250) was generated using roughness elements on the wind tunnel floor and horizontal rods and plates of various heights and spacing placed at the test section inlet. The distribution of the ABL generators can be seen in Figure 4.

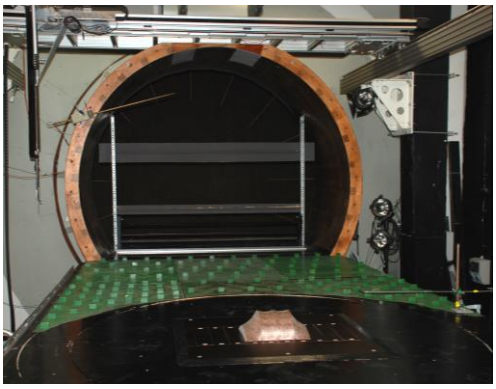

Figure 4: The 4-bay model and the ABL generators in the wind tunnel

The ABL simulation followed the criteria given by the EN 1991-1-4 [10] for the terrain category II. The profiles of the mean velocity and the velocity fluctuations are presented in Figure 5 (the values were recorded at 500 mm (~ 4 h) upstream distance from the centre of the test section). The wind tunnel test was run at $u_h \approx 11.6\,\mathrm{m/s}$ mean wind velocity ($Re = 8.7 \cdot 10^4$), after a *Re*-number dependency test run up to $18\,\mathrm{m/s}$ ($Re = 1.3 \cdot 10^5$).

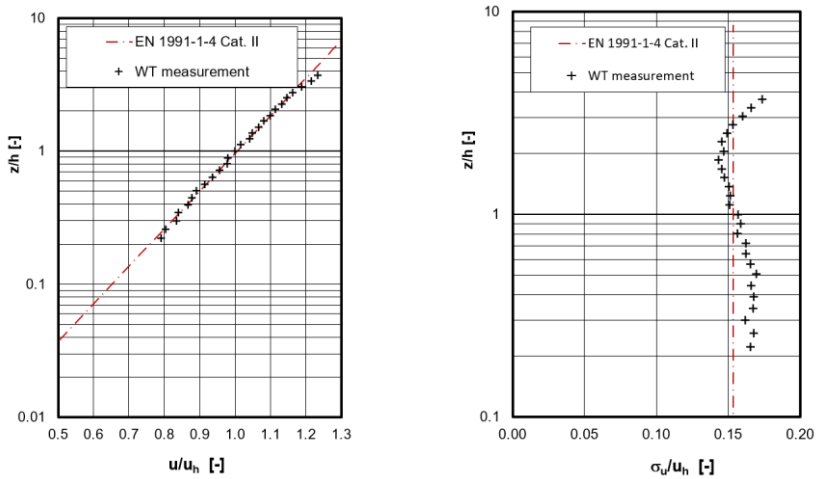

Figure 5: EC-based and in WT measured profiles of mean velocity and velocity fluctuations

3. Computational Fluid Dynamics analysis

The CFD investigation analysed the flow over the complex tensile membrane surface in ABL according to EN1991-1-4 for terrain category II (Figure 5) by assuming an incompressible fluid with constant viscosity, which is a reasonable consideration for wind engineering applications.

The applied semi-structured meshes (Figure 6) were built in Ansys Fluent. All three models were analysed using M=1:1 and M=1:250 scales. Table 1 presents the main parameters of the applied meshes.

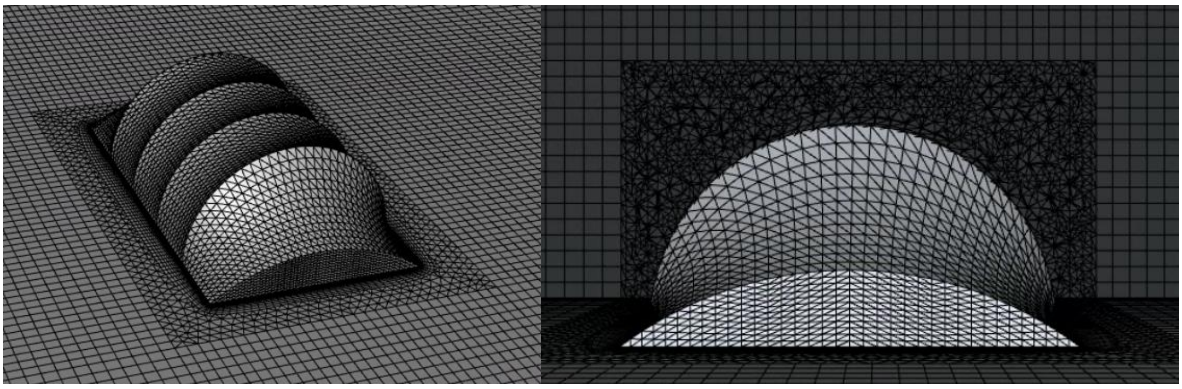

Figure 6: Numerical model and mesh around the surface

Table 1: Mesh parameters in the case of the various CFD models

	CFD model, M=1:250			CFD model, M=1:1		
	3-bay	4-bay	5-bay	3-bay	4-bay	5-bay
total cells	1 131 494	1 211 629	1 290 755	3 809 398	4 065 111	4 319 172
total nodes	1 025 138	1 080 856	1 136 430	3 511 666	3 697 614	3 883 222
elements on the membrane	2 592	3 456	4 320	2 592	3 456	4 320

The applied boundary conditions and the domain dimensions in the M=1:250 scale are shown in Figure 7. The above-introduced mean velocity and velocity fluctuations profiles were applied to the numerical model's inlets. While the flow is perpendicular to or parallel to the axis of the structure (0° and 90° wind directions), the parallel boundaries were defined as symmetry planes. In the oblique wind directions, two velocity inlets and pressure outlets were defined, according to Figure 7. This definition of the boundaries did not require the model's rotation and the remeshing of the domain for every analysed wind direction. The lower boundary (ground) and the membrane surface were defined as walls with no-slip conditions. The upper boundary is a symmetry plane.

The CFD calculations are based on the equation of continuity (conservation of mass) and the Navier-Stokes equations (conservation of momentum). There are various methods for the simulation of turbulence, from the direct numerical simulation (DNS) to the Reynolds-averaged Navier–Stokes (RANS) method. DNS solves the above-mentioned system of equations without any simplifications (resolves all turbulent eddies), providing the most precise solution besides extremely high computational demand. The RANS method models all turbulent eddies, decreasing the simulation cost to an acceptable level for practical CFD calculations. The present study applied RANS analysis, which utilizes the Reynolds decomposition of the field variables and solves the time-averaged flow equations. The decomposition results in additional terms in the momentum equations, known as Reynolds stresses. Different turbulence models can be applied, describing the above-mentioned additional terms in the function of the mean flow variables. The individual turbulence models have their strengths and weaknesses. Considering the doubly curved surface, the applied turbulence model in the current research was the k-ω Shear Stress Transport (SST) model, based on the proper combination of the standard k-ε and k-ω models, applying different blending functions. This mixed version combines the strength of the individual models, resulting in a turbulence description that is less sensitive to the boundary conditions and more capable of determining the flow separation accurately, resulting in a powerful and robust model.

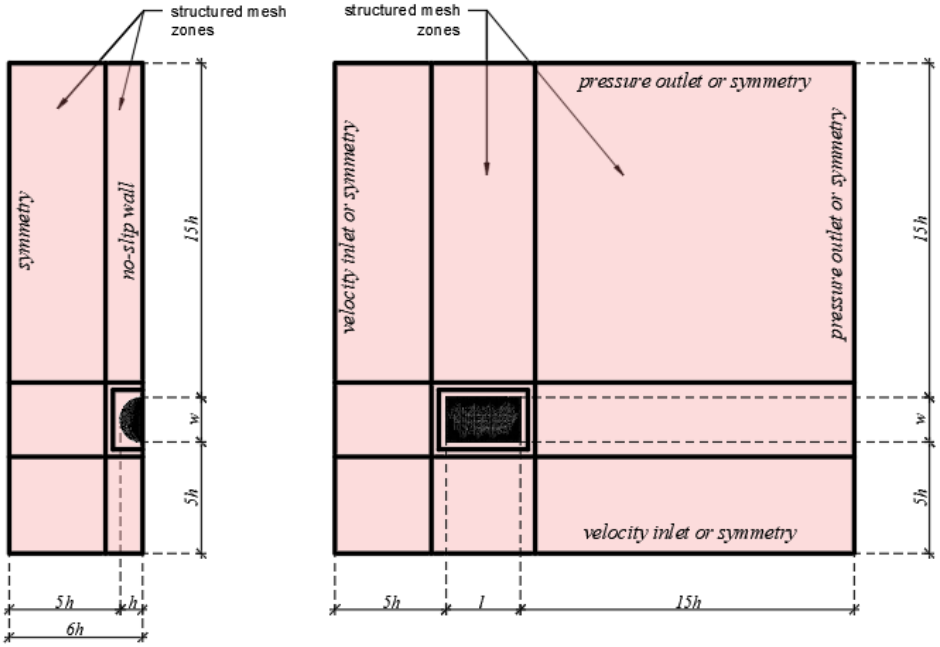

Figure 7: Dimensions of the domain and the boundary conditions (*h, w* and *l* are the height, width and length of the model)

4. Results

For the presentation of the wind load distributions according to various wind directions, the dimensionless pressure coefficient parameter at a given point of the surface at time *t* is defined as:

$$c_p(t) = \frac{p(t)-p_0}{\overline{q}_h} = \frac{p(t)-p_0}{0.5\rho_{Air}\overline{u}_h^2} \tag{1}$$

where $p(t)$ is the static pressure time series at the surface point, p_0 is the undisturbed static pressure, $\overline{q}_h$ is the mean dynamic pressure measured at the model's height, ρ_{Air} is the air density, and $\overline{u}_h$ is the streamwise mean velocity measured at the model's height. Figures 8, 9 and 10 compare the experimental and the CFD-based mean pressure coefficient ($\bar{c}_p$) maps, Tables 2, 3 and 4 present the maximum and minimum $\bar{c}_p$ values for 0°, 45° and 90° wind directions for the models with three various lengths.

The non-dimensional wind force coefficient is defined as:

$$\bar{c}_z = \frac{\bar{F}_z}{\overline{q}_h A_{xy}} = \frac{\sum \bar{c}_{pi} A_i \underline{n_i}^T \underline{e_z}}{A_{xy}}, \tag{2}$$

where $\bar{F}_z$ is the vertical component of the mean resultant wind force acting on the membrane roof, A_{xy} is the projected area of the surface to the horizontal *xy* plane, $\bar{c}_{pi}$ is the mean pressure coefficient at the i^{th} triangular membrane element, A_i is the surface area of the i^{th} triangular surface element, $\underline{n_i}$ is the unit normal vector of the i^{th} triangular element (pointing into the surface), and $\underline{e_z}$ is the unit vector in the global *z* direction. The $\bar{c}_z$ wind force coefficient was calculated for every bay separately because they are significant values during the static analysis of the membrane between the supporting arches. Figure 11 presents the WTT and CFD-based wind force coefficients of the five bays of the largest model for various wind directions. The differences between the numerical and experimental results are plotted in Figure 12.

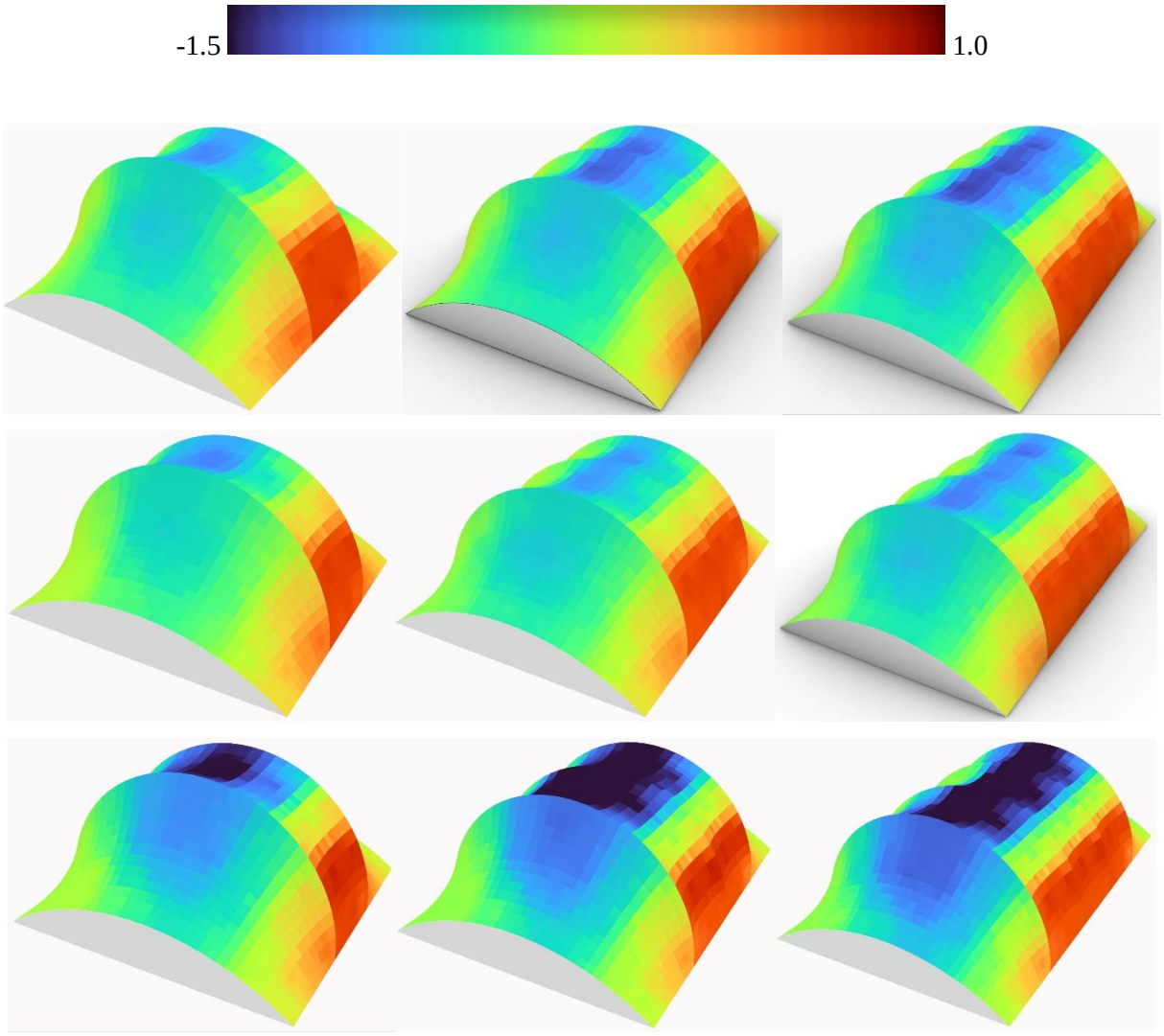

Figure 8: Mean pressure coefficient maps for 0° wind direction for the three structures based on: WTT (top row), M=1:250 CFD model (middle row) and M=1:1 CFD model (bottom row)

Table 2: Minimum and maximum values of the mean pressure coefficients

0°	3bay		4bay		5bay	
	min.	max.	min.	max.	min.	max.
WTT	-1.09	0.66	-1.24	0.67	-1.33	0.62
CFD, M=1:250	-1.11	0.65	-1.12	0.63	-1.18	0.64
CFD, M=1:1	-1.67	0.76	-2.13	0.76	-1.92	0.69

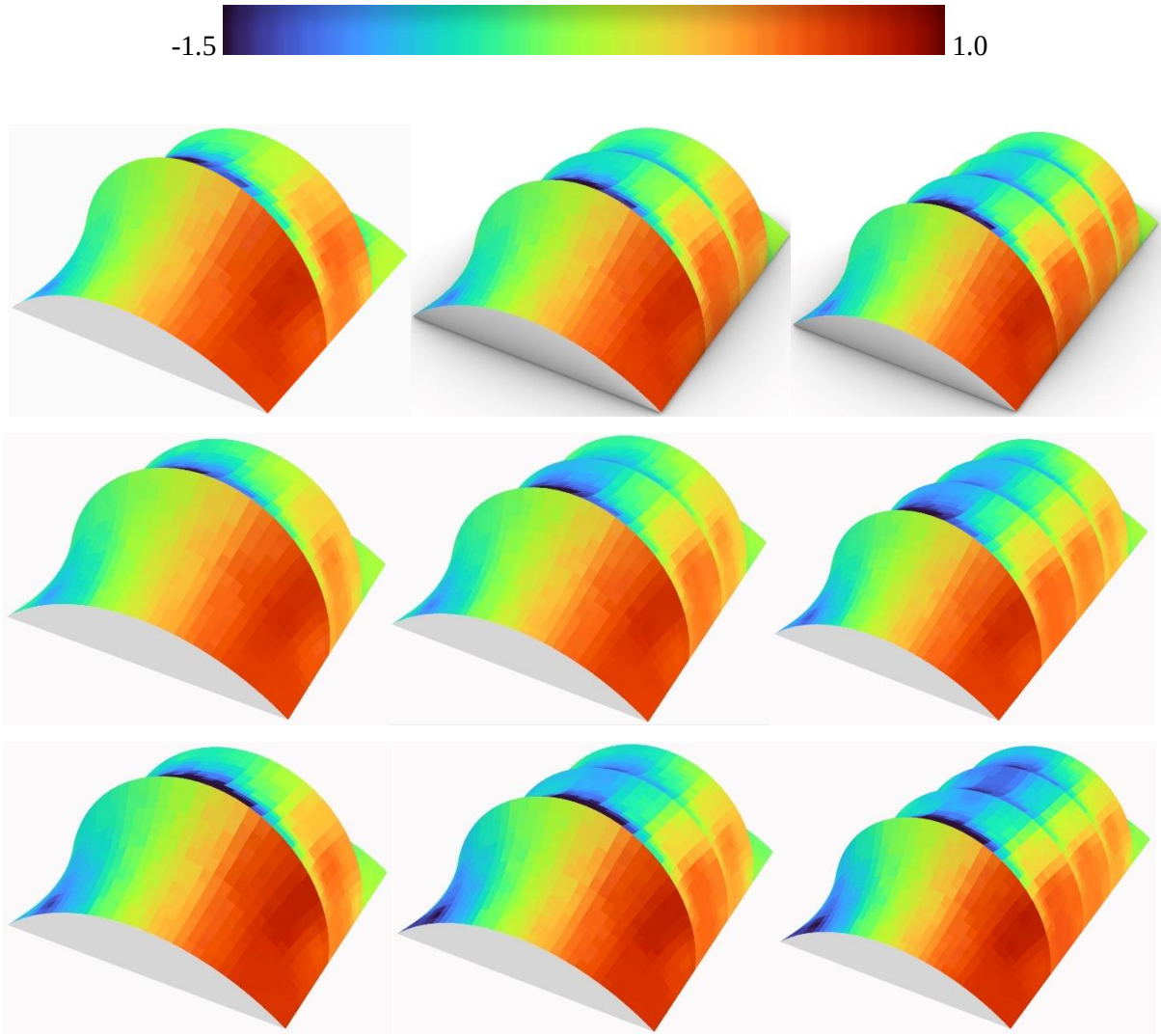

Figure 9: Mean pressure coefficient maps for 45° wind direction for the three structures based on: WTT (top row), M=1:250 CFD model (middle row) and M=1:1 CFD model (bottom row)

Table 3: Minimum and maximum values of the mean pressure coefficients

45°	3bay		4bay		5bay	
	min.	max.	min.	max.	min.	max.
WTT	-1.78	0.74	-2.02	0.72	-2.15	0.74
CFD, M=1:250	-1.59	0.72	-1.78	0.72	-1.84	0.73
CFD, M=1:1	-2.56	0.77	-2.29	0.78	-2.18	0.79

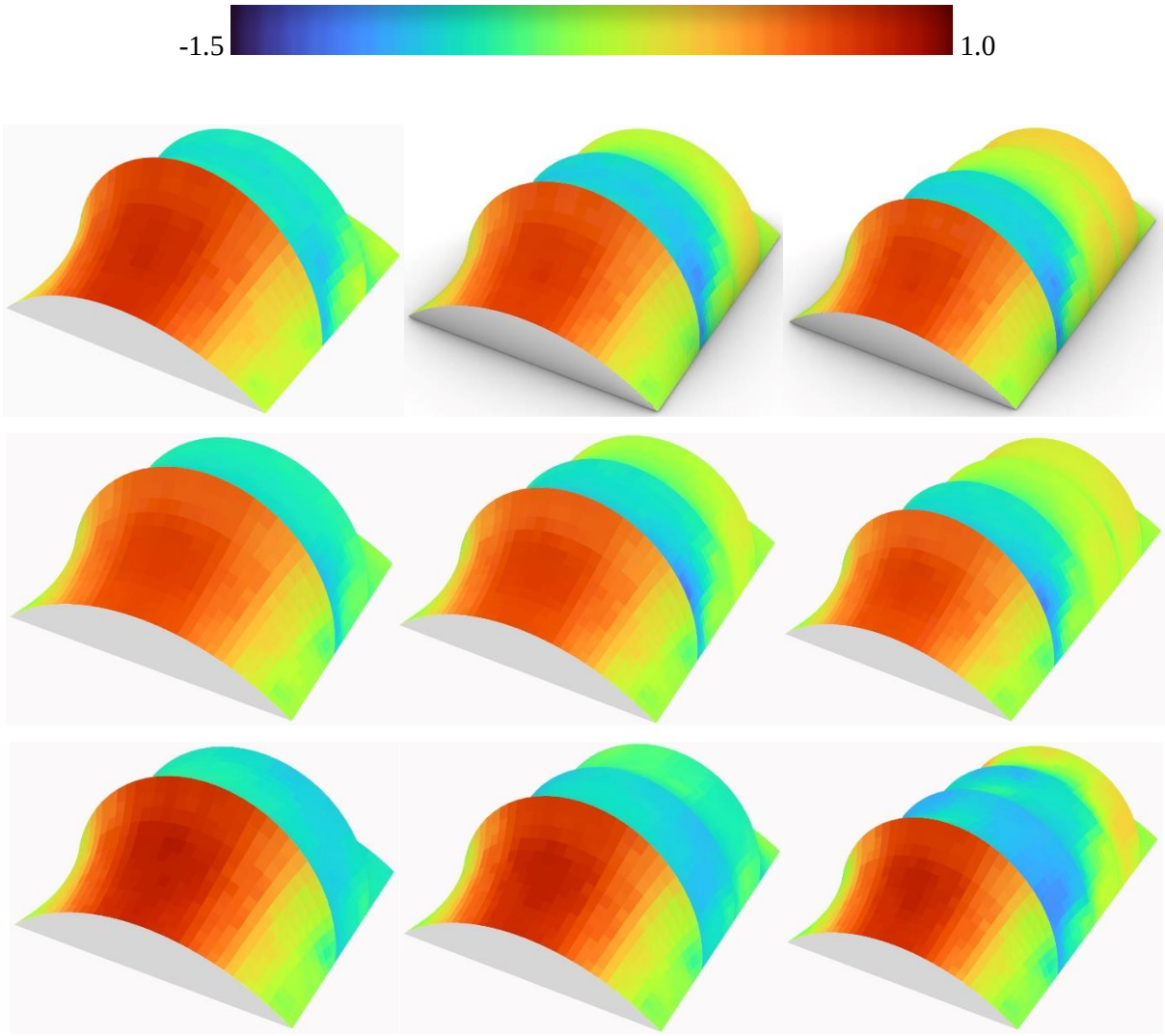

Figure 10: Mean pressure coefficient maps for 90° wind direction for the three structures based on: WTT (top row), M=1:250 CFD model (middle row) and M=1:1 CFD model (bottom row)

Table 4: Minimum and maximum values of the mean pressure coefficients

90°	3bay		4bay		5bay	
	min.	max.	min.	max.	min.	max.
WTT	-0.88	0.74	-1.05	0.66	-1.03	0.66
CFD, M=1:250	-0.90	0.62	-1.15	0.61	-1.11	0.61
CFD, M=1:1	-0.83	0.80	-0.87	0.78	-1.06	0.77

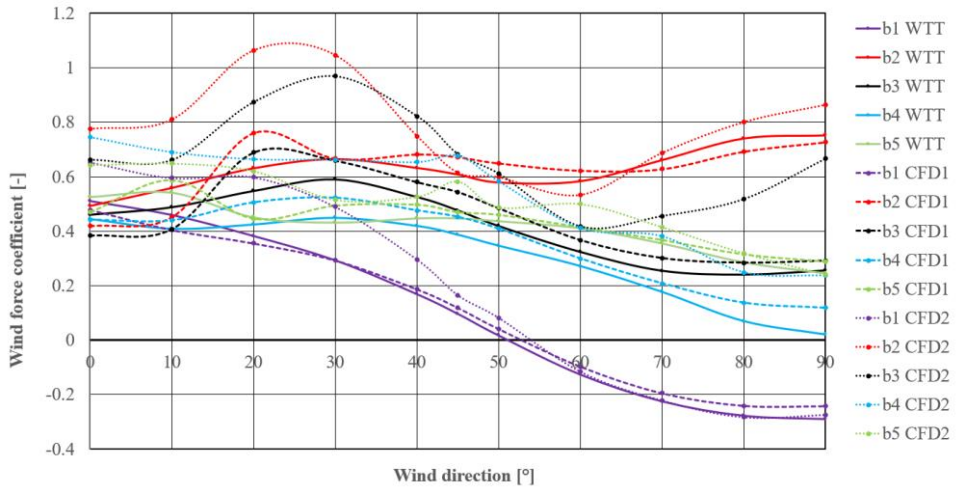

Figure 11: Characteristic values of the $\bar{c}_z$ wind force coefficients for the five bays of the largest structure for various wind directions based on the WTT (continuous lines), on the CFD analysis of the M=1:250 model (dashed line, CFD1) and on the CFD analysis of the M=1:1 model (dotted line, CFD2)

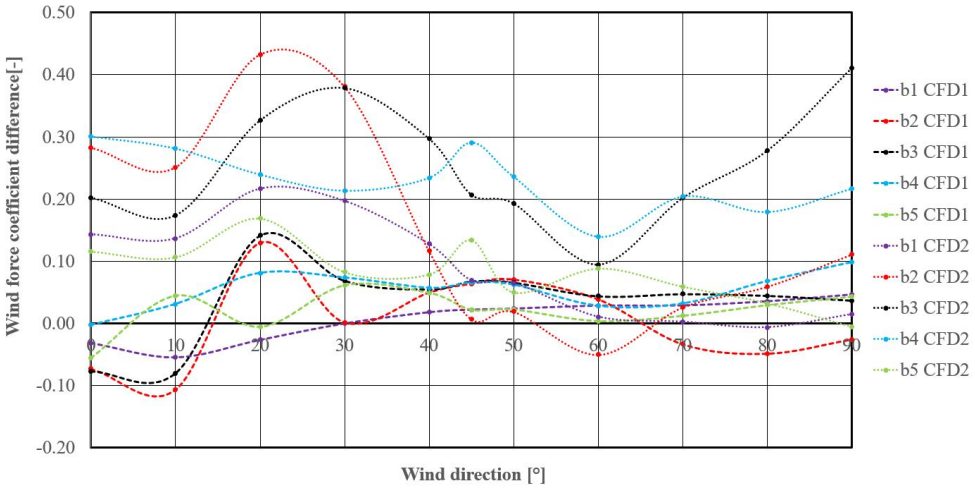

Figure 12: Differences between the CFD-based (M=1:250 model, dashed lines, M=1:1 model, dotted lines) and the experimental wind force coefficients for the five bays of the largest structure for various wind directions

To compare the numerical and experimental results, Mean Absolute Error (*MAE*)

$$MAE = \frac{1}{5}\sum_{i=1}^{5}\left|\bar{c}_{z,i(CFD)} - \bar{c}_{z,i(WTT)}\right| \tag{3}$$

values are calculated for all analyzed wind directions where $\bar{c}_{z,i}$ is the wind force (lift) coefficient in z direction for the i^{th} bay of the structure.

Table 5: *MAE* values for all analysed wind directions according to the two differently scaled numerical models and the average values of the 11 wind directions

	0°	10°	20°	30°	40°	45°	50°	60°	70°	80°	90°	Average
M=1:250	0.05	0.06	0.08	0.04	0.05	0.05	0.05	0.03	0.03	0.05	0.05	0.05
M=1:1	0.21	0.19	0.28	0.25	0.17	0.14	0.11	0.08	0.10	0.11	0.15	0.16

5. Conclusion

The research provides the experimental and CFD-based $\bar{c}_p$ pressure coefficient maps for a set of arch-supported tensile membrane structures for various wind directions. Besides the pressure coefficient distributions, the $\bar{c}_z$ wind force coefficients for every bay of the models are also presented for the various models and wind directions. The $\bar{c}_z$ wind force coefficients can be used directly during the structural analysis of membrane structures with similar shapes. Based on the comparison of the experimental and numerical results, the following conclusions are drawn:

The CFD analysis using *k-ω* SST turbulence closure of the M=1:250 scaled model provided a closer solution to the WTT than the M=1:1 numerical model. The average *MAE* value (the differences between the WTT and CFD-based results) calculated from 11 analysed wind directions was 0.05 versus 0.16.

The maximum positive (upward) WTT-based wind force coefficient was 0.75, and it was detected in the case of a wind parallel to the central axis of the model (at 90° wind direction) at the second bay in wind direction. This value was 3% smaller in the case of the M=1:250 scaled CFD model and almost 15% larger in the case of the M=1:1 scaled CFD model.

The maximum negative (downward) WTT-based wind force coefficient was -0.29, and it was also detected in the case of a wind parallel to the central axis of the model (at 90° wind direction) at the first (windward side) bay. The absolute value of the negative wind force coefficient was 16% and 5% smaller for the M=1:250 and M=1:1 scaled CFD models. It is interesting that the two load cases with constant c_p=-0.7 and c_p=0.3 on the whole surface given by The European Standard: Temporary structures - Tents – Safety [3] results in almost the same wind force coefficient as the WTT-based maximum values.

Acknowledgements

This work was supported by NKFI under Grant K138615, and VEKOP-2.3.3-15-2017-00017 project “Establishment of an Atmospheric Flow Laboratory”.

References

[1] M. R. Barnes, “Form-finding and analysis of prestressed nets and membranes,” *Computers and Structures*, vol. 30, pp. 685-695, 1988.

[2] K. Hincz, “Determination of the cutting patterns of prestressed tent structures,” *Revista Portuguesa de Engenharia de Estruturas*, vol. 47, pp. 45-49, 2000.

[3] Eurocode, EN 13782:2005: Temporary structures - Tents - Safety. CEN, European Committee for Standardization, Brussels, Belgium, 2005

[4] B. Forster, M. Mollaert (eds.), *European Design Guide for Tensile Surface Structures*, TensiNet, 2004.

[5] R. P. Hoxey, G. M. Richardson, “Measurements of wind loads on full-scale film plastic clad greenhouses,” *Journal of Wind Engineering and Industrial Aerodynamics*, vol. 16, pp. 57-83, 1984.

[6] F. Rizzo, M. Barbato, V. Sepe, “Peak factor statistics of wind effects for hyperbolic paraboloid roofs,” *Engineering Structures*, vol. 173, pp. 313-330, 2018.

[7] X. Sun, K. Arjun, Y. Wu, “Investigation on wind tunnel experiment of oval-shaped arch-supported membrane structures,” *Journal of Wind Engineering and Industrial Aerodynamics*, vol. 206, art. no. 104371, 2020.

[8] K. Hincz, M. Gamboa-Marrufo, “Deformed Shape Wind Analysis of Tensile Membrane Structures,” *Journal of Structural Engineering*, vol. 142(3), art. no. 04015153, 2016.

[9] A. S. Day, “An introduction to dynamic relaxation”, *The Engineer*, vol. 219, pp. 218-21, 1965.

[10] Eurocode, EN 1991-1-4:2005 Eurocode 1: Actions on structures - Part 1-4: General actions - Wind actions. CEN, European Committee for Standardization, Brussels, Belgium, 2010